JOURNAL OF SPACECRAFT AND ROCKETS
Vol. 34, No. 6, November–December 1997

Model of Plasma Contactor Performance

I. Katz,* B. M. Gardner,† M. J. Mandell,‡ and G. A. Jongeward§
Maxwell Technologies, San Diego, California 92123-1506
M. Patterson¶
NASA Lewis Research Center, Cleveland, Ohio 44135
and
R. M. Myers**
Olin Aerospace Company, Redmond, Washington 98073-9709

A hollow cathode-based plasma contactor will be flown on the international space station to control the station's potential to within ±40 V of the local ionosphere. Extensive testing of the plasma contactor has been conducted in vacuum facilities at the NASA Lewis Research Center. Significant performance differences were observed between tests of the same plasma contactor in different facilities. Why measured plasma contactor performance differs in the laboratory in different tank environments and how the plasma contactor performance measured in the laboratory relates to expected performance in space is addressed. Presented are models of plasma contactor plasma generation and interaction in a laboratory environment, including anode area limiting. These models were integrated using the Space Station Environment Work Bench to predict plasma contactor operation, and the results are compared with the laboratory measurements.

Nomenclature

F = gas flow rate, standard cubic centimeter per minute
I_D = total orifice electron current, A
I_{emission} = orifice current emitted, A
I_{keeper} = keeper electrode current, A
I_{loss} = ion loss rate, A
$I_{\max}$ = maximum possible electron current, A
I_{prod} = total ion production rate, A
J_e = electron current density, A m^{-2}
L = orifice length, m
m = neutral atom mass, kg
m_e = electron mass, kg
m_i = ion mass, kg
N_n = neutral density, m^{-3}
r = orifice radius, m
W_{conv} = power loss by electron convection, W
W_{ion} = power loss by ionization, W
W_{rad} = power loss by radiation, W
θ_e = orifice electron temperature, eV
θ_i = ion temperature, eV
θ_{in} = insert region electron temperature, eV
θ_n = neutral gas temperature, eV
σ = electrical conductivity, ohm m^{-1}
σ_{ion} = ionization cross section, m^{-3}
σ_{rad} = inelastic cross section, m^{-3}
ω_p = electron plasma frequency, rad s^{-1}

Introduction

THE solar arrays on the international space station (ISS) generate up to 160 V. The negative terminals of the arrays are connected to the space station ground. Because the solar arrays collect electrons from the ionosphere, the array voltage will drive the space station ground over 100 V negative with respect to the ionosphere.[1] Laboratory tests have shown that at these voltages, space station anodized coatings would arc, and their thermal control properties would degrade.[2–4] To prevent this arcing, a hollow cathode-based plasma contactor (PC) will be flown on the ISS to control the station's potential within ±40 V of the local ionosphere. The hollow cathode is based on ion thruster neutralizer technology developed by the On-Board Propulsion Branch of the NASA Lewis Research Center (LeRC). Extensive testing of the PC has been conducted in vacuum facilities (VF) at NASA LeRC. Significant performance differences were observed between tests of the same PC in VF 5 and VF 11. This paper addresses why measured PC performance differs in the laboratory in different tank environments. A model of PC plasma generation[5] and interaction, including anode limiting and plume expansion, has been integrated into the Environment Work Bench (EWB)[6] to predict PC operation both in the laboratory and in space. Calculations show that the results obtained in VF 5 and VF 11 are both consistent with the PC plasma generation model.

VF 11 and VF 5 Measurements

The ISS PC is being designed to emit up to 10 A of electrons into the ionosphere at a potential difference between the ionosphere acting as anode and the PC cathode, commonly referred to as the clamping potential, of less than 20 V. Tests of a prototype enclosed keeper hollow cathode PC were conducted in VF 5. VF 5 is a very large steel vacuum chamber whose walls, acting as the anode here, make a good electrical contact with the PC-generated plasma. The tests showed that the clamping potential requirement was easily met with a 6.0-standard cubic centimeter per minute (sccm) flow rate and 2.0 A flowing in the circuit between the cathode insert and the keeper electrode. The current in this circuit is designed to keep the discharge alive when no other currents are flowing. Higher keeper currents provide additional ionization and increased emission current capability.

VF 11 is a smaller chamber made from aluminum. Aluminum oxide forms on the walls and prevents a good electrical contact with the PC-generated plasma. Stainless steel anode plates line the chamber walls to enable electrical contact with the plasma. The stainless steel plates cover more than 70% of the chamber walls. Tests of the PC in the VF 11 chamber resulted in anode potentials in excess of 20 V for all emission currents above 5 A, even with a 3.0-A keeper current. Subsequent measurements of plasma potentials in VF 11 showed that the potential between the PC and the surrounding

Received Dec. 20, 1996; revision received May 17, 1997; accepted for publication May 23, 1997.

*Vice President, Maxwell Federal Division, 8888 Balboa Avenue. Member AIAA.
†Staff Scientist, Maxwell Federal Division, 8888 Balboa Avenue. Member AIAA.
‡Senior Staff Scientist, Maxwell Federal Division, 8888 Balboa Avenue. Senior Member AIAA.
§Vice President, Sector Manager, Contract Research, Maxwell Federal Division, 8888 Balboa Avenue.
¶Aerospace Engineer, 21000 Brookpark Road.
**Director, Electric Propulsion, PRIMEX Aerospace, P.O. Box 97009.

plasma was less than 20 V. The additional potential drop was across the sheath surrounding the stainless steel anode plates.

Both chambers are specially designed for testing electric propulsion systems and have very large cryopumps. Facility pressures during PC operation were consistently below 10^{-5} torr for both tanks. In the following we discuss the reason for the difference in anode potentials in the two chambers and present an analysis procedure to extrapolate the laboratory PC test results to predict on-orbit performance.

Review of PC Plasma Generation

Figure 1 shows the typical dimensions of a hollow cathode PC for space applications. Though the entire device is fairly small, the orifice through which the insert region communicates with the external space is an order of magnitude smaller still. As this region has an extremely high-current density, processes taking place in the orifice region govern the amount of plasma flowing from the device.

The operation of hollow cathodes has been investigated in the laboratory.[5] Previous studies[7–9] have analyzed the physical processes inside the hollow cathode, which lead to electron emission from the insert. We present a simple model of the ionization and energy balance in the orifice of a hollow cathode. The model is consistent with previous models of the physics interior to the hollow cathode but investigates in more detail what occurs within the tiny orifice region.

Model of Orifice Processes

The orifice is so small that, although it is many times larger than the plasma debye length, it extends for only a few mean free paths for electrons, ions, or neutrals. Therefore, it is reasonable to treat the orifice as a cylinder containing a homogeneous neutral plasma with a thin wall sheath. Known are the gas flow through the device; the total discharge current through the orifice, I_D; and the temperature of the electrons entering from the insert region θ_{in}. The discharge current I_D is the sum of the emission current and the keeper current. We will calculate the electron temperature and plasma density in the orifice, the plasma output of the device, the voltage required to sustain the discharge current through the orifice, and the energy budget of the orifice region.

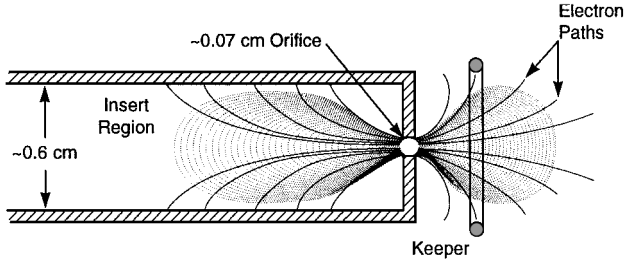

Fig. 1 Typical dimensions of a hollow cathode for space applications.

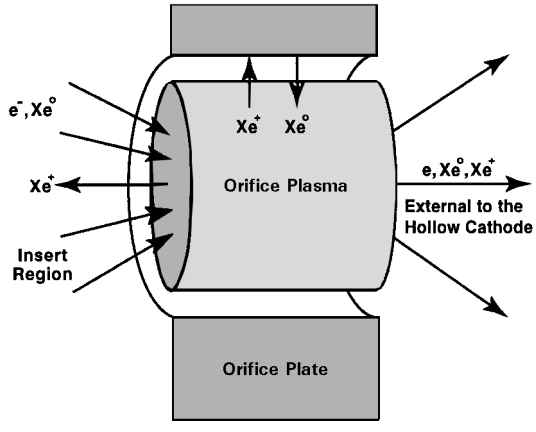

Fig. 2 Magnified view of the cylindrical orifice region as modeled.

Electron Temperature

Figure 2 shows a schematic view of the orifice region with xenon atoms and electrons entering from the insert region; xenon ions flowing back to the insert region; electrons, xenon atoms, and xenon ions being emitted to the external plasma; and xenon ions recombining at the orifice walls to form xenon neutral atoms. To have a steady-state plasma in the orifice, the electrons must be sufficiently hot to create ions at a rate equal to the loss of ions to the orifice wall and by flow out the ends. We assume the following in the orifice.

1) The neutral gas density N_n is known.

2) The electron energy distribution is Maxwellian with temperature θ_e.

3) The ions are accelerated toward the orifice boundaries by quasineutral electric fields. We approximate this by assuming $\theta_i = \theta_e$.

4) The plasma is quasineutral, so that $n_i = n_e = n$.

For a cylindrical orifice of radius r and length L, the ion production rate in amperes, I_{prod}, is given by

$$I_{\text{prod}} = \pi r^2 L \times 4\sigma_{\text{ion}}(\theta_e) \times J_e N_n \tag{1}$$

where $\sigma_{\text{ion}}(\theta_e)$ is the thermally averaged cross section for electron impact ionization of xenon[10] found by integrating the energy-dependent cross section over a Maxwellian distribution. For temperatures up to several electron volts, the temperature-averaged cross section is well fit by

$$\sigma_{\text{ion}}(\theta_e) = \left[3.97 + 0.643\theta_e - 0.0368\theta_e^2\right] e^{-12.127/\theta_e} \times 10^{-20}\ \text{m}^2 \tag{2}$$

$J_{e,i}$ is the electron or ion thermal current density

$$J_{e,i} = ne\left(\frac{e\theta_{e,i}}{2\pi m_{e,i}}\right)^{\frac{1}{2}} \tag{3}$$

The neutral density is calculated by assuming the flow rate equals the thermal flux through the orifice cross-sectional area,

$$\pi r^2 \times eN_n(e\theta_n/2\pi m_n)^{\frac{1}{2}} = (0.0718F - I_I) \tag{4}$$

where I_I is the ion output of the device in amperes. The ion loss rate is given by

$$I_{\text{loss}} = 2\pi r(r + L)J_i \tag{5}$$

Solving Eqs. (1–5) results in an electron temperature in the orifice of about 2 eV for a wide range of hollow cathode parameters. Figure 3 shows electron temperature in the orifice as a function of gas flow rate. The two curves correspond to ion temperature of 0.1 eV (lower curve) and ion temperature equal to electron temperature (upper curve). In the limiting case where the ion production is negligible

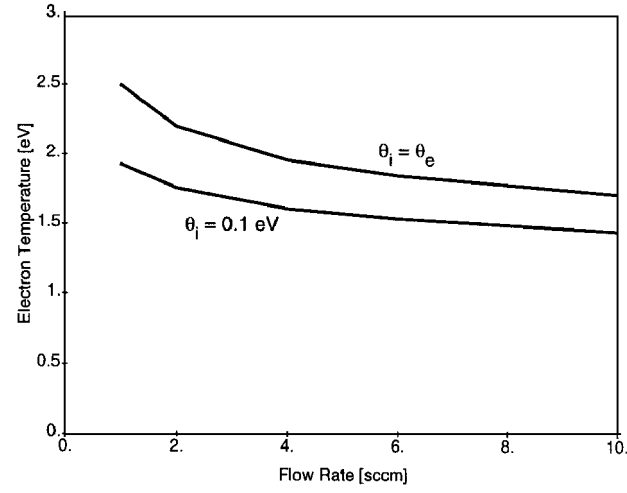

Fig. 3 Orifice electron temperature in the orifice as a function of gas flow rate.

compared with gas flow, the electron temperature is independent of plasma density and depends only weakly on the gas flow rate and the ion and neutral temperatures.

Electrical Resistance

Plasma conductivity σ is given by

$$\sigma = \varepsilon_0 \omega_p^{2/\nu} \qquad \omega_p^2 = ne^2/\varepsilon_0 m_e \tag{6}$$

where ν is the effective scattering rate for conduction. The scattering rate ν is the sum of 1) electron-ion scattering

$$\nu_{ei} = 2.9 \times 10^{-12}\, n_e \Lambda \theta_e^{-\frac{3}{2}} \tag{7}$$

and 2) electron-neutral scattering

$$\nu_{en} = 5 \times 10^{-19}\, N_n (e\theta_e/m)^{\frac{1}{2}} \tag{8}$$

The quantity Λ, the coulomb logarithm, given by

$$\Lambda = 30 - \tfrac{1}{2}\, \ell n \left(n_e \theta_e^{-3}\right) \tag{9}$$

is about 7 for the orifice conditions. We neglect any nonclassical scattering. The electrical resistance R of the orifice is then

$$R = L/\pi r^2 \sigma \tag{10}$$

Ohm's law is used to relate the total orifice discharge current I_D to the voltage across the orifice $I_D R$ and the power dissipated in the orifice $I_D^2 R$.

Energy Loss Mechanisms

There are three major energy-loss mechanisms for the electron gas in the orifice region. Xenon atoms, excited or ionized by electron collisions, either radiate to the external world, leaving the orifice, or are quenched at the walls. These processes are the major loss mechanisms. Another significant loss is by electron convection, which is simply a statement that the insert electron temperature is cooler than the orifice electron temperature. The expressions for these losses follow.

1) Ionization loss:

$$W_{ion} = \langle E_{ion} \rangle \times I_{prod} \tag{11}$$

where $\langle E_{ion} \rangle$ is the mean energy loss due to an ionization event (taken to be 12.2 eV for xenon).

2) Radiation loss:

$$W_{rad} = \pi r^2 L \times \langle E_{rad} \rangle \times 4\sigma_{rad}(\theta_e) \times J_e N_n \tag{12}$$

where $\langle E_{rad} \rangle$ is the mean energy loss due to an excitation event, taken to be about 10 eV, because for xenon even the lowest lying excited state is 8.5 eV above ground. The Maxwellian averaged cross-section for xenon radiative excitation,[9] $\sigma_{rad}(\theta_e)$, is approximated for electron temperatures of a few electron volts by

$$\sigma_{rad}(\theta_e) \sim 1.93 \times 10^{-19} \theta_e^{-\frac{1}{2}} - e^{-11.6/\theta_e} \tag{13}$$

3) Convective loss:

$$W_{conv} = I_D(\theta_e - \theta_{in}) \tag{14}$$

where θ_{in} is the electron temperature at the input to the orifice from the insert region. Based on the work of Salhi and Turchi,[8] we assume the entering electrons to have a temperature of 1 eV.

The orifice plasma density is found by balancing the ohmic heating with the sum of the three energy losses,

$$I_D^2 R = W_{ion} + W_{rad} + W_{conv} \tag{15}$$

Results

Equations (1–15) are used in EWB to calculate self-consistently the plasma density, electron temperature, power dissipation, and ion output $I_{ion} = (\pi r^2 J_i)$ of the orifice as a function of orifice dimensions, gas flow rate, and discharge current. The calculation consists of iterating the orifice plasma temperature and density until the ion production equals the ion loss and the I^2R power dissipation in the orifice equals the total energy loss. The maximum electron current I_{max} that can flow through the orifice is the one-sided electron thermal current times the ion current[11]

$$I_e^{max} = \sqrt{(m_i/2\pi m_e)}\, I_{ion}$$

VF 5 Operations

Table 1 shows the calculated I_{max} as a function of PC emission current ($I_{emission} = I_D - I_{keeper}$) for xenon flow rates of 6.0 and 7.5 sccm and a keeper current of 2 A. The calculations were done using the PC model in EWB.

The EWB model indicates that, for $I_{keeper} = 2.0$ A, even at 6.0 sccm, the PC can support all emission currents between 0 and 11 A, that is,

$$I_{emission} < I_{max}$$

for

$$0 < I_{emission} < 11\ \text{A}$$

These results are consistent with measurements made in VF 5, as shown in Fig. 4. That is, the PC emitted up to 10 A at less than 20-V clamping potentials.

Note that the model shows that an increase of 1 A of keeper current is more effective in generating plasma than is a 1-sccm increase in xenon flow rate. (The ISS PC will operate at 3 A not 2 A. This increase in keeper current was to address long-term cathode temperature/stability issues, not to increase emission capabilities.) During the same test sequence, the PC was operated at a low, 3.8-sccm,

Table 1 Calculated I_{max} as a function of PC emission current for flow rates of 6.0 and 7.5 sccm

$I_{emission}$	I_{max}, 6 sccm	I_{max}, 7.5 sccm
0.00	1.14	1.24
1.00	1.79	1.96
2.00	2.52	2.75
3.00	3.29	3.58
4.00	4.12	4.50
5.00	5.16	5.49
6.00	6.20	6.70
7.00	7.33	7.86
8.00	8.32	9.17
9.00	9.31	10.23
10.00	10.54	11.48
11.00	11.75	12.54

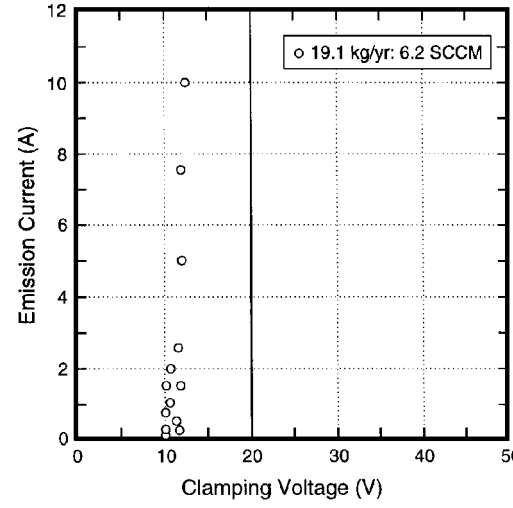

Fig. 4 PC current voltage characteristics with 6.2-sccm gas flow rate as measured in VF 5.

Table 2 Calculated I_{max} as a function of PC emission current for a 3.8-sccm flow rate

$I_{emission}$	I_{max}, 3.8 sccm
0.00	0.92
1.00	1.47
2.00	2.06
3.00	2.69
4.00	3.52
5.00	4.35
6.00	5.19
7.00	5.96
8.00	6.81
9.00	7.70
10.00	8.54
11.00	8.96

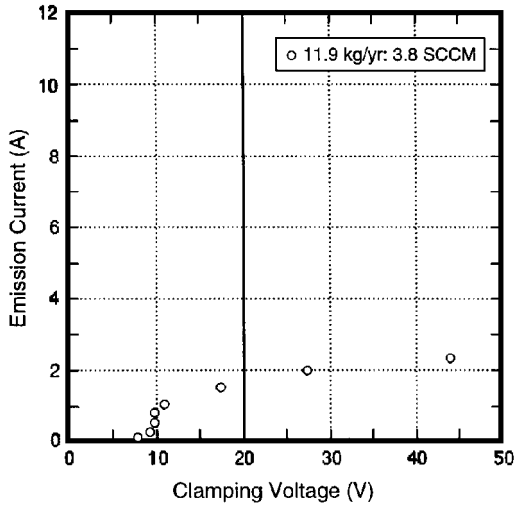

Fig. 5 PC current voltage characteristics with 3.8-sccm gas flow rate as measured in VF 5.

flow rate and proved unable to emit more than 2.5 A, even for 50-V clamping potentials, as shown in Fig. 5.

Table 2 shows the EWB calculation for the 3.8-sccm xenon flow rate. The EWB model predicts maximum emission currents as a function of emission current for a keeper current of 2.0 A. The emission current has to be less than I_{max} for the PC to operate in a low-impedance mode. For example (Table 2), the plasma generated assuming an emission current of 8 A is only able to support a maximum emission current of 6.81 A. Because 8 A of emission current was assumed, the solution is not self-consistent. Thus, the plasma generated cannot support the current without large potentials. For the 2.0-A keeper current used in the test, the model predicts that only for

$$I_{emission} < 2\,\text{A}$$

would the PC emission current not exceed the maximum PC current.

At higher emission currents, the electron drift velocity exceeds the electron thermal velocity, and the plasma would be highly resistive. Comparing the EWB model with the laboratory results, the EWB model predicts about the same I_{max} as observed.

Partial Anode Operations: VF 11

Tests performed in VF 11 using the same PC, but operating at an increase to 3-A keeper current (Fig. 6), showed higher clamping potentials when the potential was measured between the PC and the chamber walls. This potential increase is consistent with sheath formation at the anode plates. When the one-sided plasma electron thermal current over the anode surface is less than the required current, the increase in voltage forms a sheath around the anode plate. The sheath has a surface area larger than the anode plate and collects more current.

Based on a relatively simple EWB geometrical model, we calculate that in VF 11 the anode plates intercept approximately 70% of the PC plume. This implies that the maximum current the PC can emit in VF 11 at low voltages is about 70% of what it can emit in VF 5. The calculation shown in Table 3 predicts high-voltage sheaths will form for emission currents above 2 A. The EWB model appears to predict a slightly larger emission current capability than was measured in the laboratory. As can be seen in Fig. 5, the voltage in the laboratory started to increase around 1 A.

Table 3 Calculated I_{max} for ideal anode and for VF 11 anode at 6.0-sccm flow rate, showing margin between emission current and VF 11 I_{max}

$I_{emission}$	I_{max}, 6 sccm	VF 11, I_{max}	Margin
0.00	1.79	1.25	1.25
1.00	2.52	1.76	0.76
2.00	3.29	2.30	0.30
3.00	4.12	2.88	−0.12
4.00	5.16	3.61	−0.39
5.00	6.20	4.34	−0.66
6.00	7.33	5.13	−0.87
7.00	8.32	5.82	−1.18
8.00	9.31	6.52	−1.48
9.00	10.54	7.38	−1.62
10.00	11.75	8.23	−1.78

Table 4 Calculated I_{max} for ideal anode and for VF 11 anode at 7.5-sccm flow rate, showing margin between emission current and VF 11 I_{max}

$I_{emission}$	I_{max}, 7.5 sccm	VF 11, I_{max}	Margin
0.00	1.96	1.37	1.37
1.00	2.75	1.93	0.93
2.00	3.58	2.51	0.51
3.00	4.50	3.15	0.15
4.00	5.49	3.84	−0.16
5.00	6.70	4.69	−0.31
6.00	7.86	5.50	−0.50
7.00	9.17	6.42	−0.58
8.00	10.23	7.16	−0.84
9.00	11.48	8.04	−0.96
10.00	12.54	8.78	−1.22

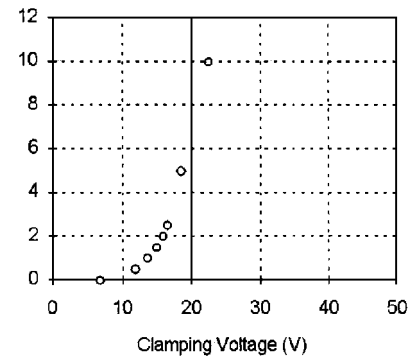

Fig. 6 PC current voltage characteristics with 6.0-sccm gas flow rate as measured in VF 11.

We also performed the same set of calculations for a higher, 7.5-sccm, xenon flow rate. The results (Table 4) indicate that sheath formation would begin at emission currents above 3 A. These calculations, although not exact, do reproduce the observed trend that the current margin deficits are higher at given emission currents at the 6.0-sccm flow rate than at the 7.5-sccm flow rate. For example, the current deficit at an emission current of 5 A for a 7.5-sccm flow rate is 0.31 A, whereas the same emission current for a 6.0-sccm flow rate yields a current deficit of 0.66 A. This implies higher sheath potentials for a 6-sccm flow rate than for the 7.5-sccm flow rate for the same emission current, as seen in the laboratory.

Conclusion

The laboratory data and the analysis confirm that the PC current-carrying capability is determined by the amount of plasma generated that actually contacts the effective anode. We have presented a

model based on conservation of mass and energy, which calculates the amount of plasma generated by a hollow cathode-based plasma contactor.

In the large laboratory chamber, the effective anode is the entire tank interior surface. The laboratory data show that, when the gas flow was reduced, PC emission currents were limited to a few amperes, even for relatively high voltages. However, at higher gas flow rates, large emission currents were observed for even low voltages. Calculations performed using the model show that, for the small gas flow rate, the PC ion production was inadequate to support high currents. However, at the higher gas flow, the PC generated sufficient ions to support much greater plasma thermal currents.

In tests in the small chamber, the effective anode is the stainless steel plates. Calculations showed that, although the plasma generated by the PC was adequate to carry many ampere emission currents, not enough of the plasma was in contact with anode surface for a low-impedance flow. This was confirmed by the measurement of anode sheath potential. The anode sheath increases the effective collecting area of the anode, but the sheath potential increases the measured clamping voltage.

Acknowledgment

This work was sponsored by NASA Contract NAS3-23881 from NASA Lewis Research Center.

References

[1]Stevens, N. J., Berkopec, F. D., Purvis, C. K., Grier, N., and Staskus, J., "Investigation of High Voltage Spacecraft System Interactions with Plasma Environment," AIAA Paper 78-672, April 1978.

[2]Carruth, M. R., Jr., Vaughn, J. A., and Gray, P. A., "Experimental Studies on Spacecraft Arcing," AIAA Paper 92-0820, Jan. 1992.

[3]Carruth, M. R., Jr., Vaughn, J. A., Holt, J. M., Werp, R., and Sudduth, R. D., "Plasma Effects on the Passive Thermal Control Coatings of Space Station Freedom," AIAA Paper 92-1685, March 1992.

[4]Vaughn, J. A., Carruth, M. R., Jr., Katz, I., Mandell, M. J., and Jongeward, G. A., "Electrical Breakdown Currents on Large Spacecraft in Low Earth Orbit," *Journal of Spacecraft and Rockets*, Vol. 31, No. 1, 1994, pp. 54–59.

[5]Mandell, M. J., and Katz, I., "Theory of Hollow Cathode Operation in Spot and Plume Modes," AIAA Paper 94-3134, 1994.

[6]Gardner, B. M., Jongeward, G. A., Kuharski, B., Wilcox, K., Rankin, T., and Roche, J., "The Environmental Workbench: A Design Tool for the International Space Station," AIAA Paper 95-0599, 1995.

[7]Salhi, A., and Turchi, P. J., "A First-Principles Model for Orificed Hollow Cathode Operation," AIAA Paper 92-3742, 1992.

[8]Salhi, A., and Turchi, P. J., "Theoretical Modeling of Orificed, Hollow Cathode Discharges," International Electric Propulsion Conf., IEPC-93-024, 1993.

[9]Siegfried, D. E., and Wilbur, P. J., "An Investigation of Mercury Hollow Cathode Phenomena," AIAA Paper 78-705, 1978.

[10]Hayashi, M., "Determination of Electron-Xenon Total Excitation Cross-Sections, from Threshold to 100 eV, from Experimental Values of Townsend's α," *Journal of Physics D: Applied Physics*, Vol. 16, 1983, pp. 581–589.

[11]Parks, D. E., Katz, I., Buchholtz, B., and Wilbur, P., "Expansion and Electron Emission Characteristics of a Hollow-Cathode Plasma Contactor," *Journal of Applied Physics*, Vol. 74, No. 12, 1993, pp. 7094–7100.

A. C. Tribble
Associate Editor